Reduction of the Wet Surface Heat Transfer Coefficients from Experimental Data

Nae-Hyun Kim†, Yong-Sub Sim*

Department of Mechanical Engineering, University of Incheon, Incheon 402-749, Korea

**Graduate School, University of Incheon, Incheon 402-749, Korea*

Key words: Wet surface, Dehumidification, Heat transfer coefficient, Data reduction, Air-side

ABSTRACT: Four different data reduction methods for the heat transfer coefficients from experimental data under dehumidifying conditions are compared. The four methods consist of two heat and mass transfer models and two fin efficiency models. Data are obtained from two heat exchanger samples having plain fins or wave fins. Comparison of the reduced heat transfer coefficients revealed that the single potential heat and mass transfer model yielded the humidity-independent heat transfer coefficients. Two fin efficiency models—enthalpy model and humidity model—yielded approximately the same fin efficiencies, and accordingly approximately the same heat transfer coefficients. The heat transfer coefficients under wet conditions were approximately the same as those of the dry conditions for the plain fin configuration. For the wave fin configuration, however, wet surface heat transfer coefficients were approximately 12% higher. The pressure drops of the wet surface were 10% to 45% larger than those of the dry surface.

Nomenclature

A : heat transfer area [m^2]
b : slope of the enthalpy-temperature curve of saturated air [kJ/kgK]
c_p : specific heat [kJ/kgK]
f : friction factor [-]
h : heat transfer coefficient [W/m^2K]
i : enthalpy [kJ/kg]
j : Colburn j-factor [-]
k : thermal conductivity [W/mK]
Le : Lewis number [-]
$\dot{m}$: mass flow rate [kg/s]
N : Number of tube row [-]
NTU : number of transfer units [-]
P : perimeter [m]
P_d : wave length [m]
P_f : fin pitch [m]
P_l : longitudinal tube pitch [m]
Pr : Prandtl number [-]
P_t : transverse tube pitch [m]
q : heat transfer [W]
r_c : tube radius including fin collar [m]
Re : Reynolds number [-]
R_{eq} : equivalent diameter of the radial fin [m]
RH : relative humidity [-]
t : thickness [m]
T : temperature [K]
U : overall heat transfer coefficient [W/m^2K]
V : air velocity in a heat exchanger [m/s]
w : absolute humidity [kg/kgair]
x : length of a heat exchanger [m]
x_f : wave depth [m]

† Corresponding author
Tel.: +82-32-770-8420; fax: +82-32-770-8401
E-mail address: knh0001@incheon.ac.kr

Greek symbols

ΔP : pressure loss [Pa]
μ : dynamic viscosity [kg/ms]
η : fin efficiency [-]
η_o : surface efficiency [-]
σ : contraction coefficient [-]

Subscripts

a : air
b : fin base
c : fin collar or cross section
d : dry
D : diameter or diffusion
db : dry bulb
f : fin
fg : liquid-vapor
i : inside
L : latent
m : mean
ma : air-steam mixture
max : maximum
min : minimum
o : outside
r : tube-side
s : surface or sensible
t : tube wall or fin tip
w : wet surface or water
wb : wet bulb
wv : steam

1. Introduction

Fin-and-tube heat exchangers are extensively used as evaporators of household or commercial air-conditioning units due to structural and manufacturing simplicity. When the fin surface temperature is lower than the dew-point temperature of the incoming air, the moisture is condensed on the fin surface. The condensed moisture releases latent heat of condensation. The wet surface heat transfer consists of the latent heat transfer and the sensible heat transfer. Traditionally, the thermal performance of wet surface has been expressed as a sensible heat transfer coefficient. The reduction of sensible heat transfer coefficient from measured parameters requires heat and mass transfer analysis. Depending on the heat and mass transfer models, the reduced heat transfer coefficients could be significantly different.

The literature shows two heat and mass transfer analysis models – single potential model and dual potential model. The single potential model assumes that the heat and mass transfer is driven by one single potential – enthalpy. In this method, the sensible heat transfer coefficient is obtained from the total heat transfer (which includes both latent heat transfer and sensible heat transfer). This model has been used by ARI.[1] In the dual potential model, the sensible heat transfer is assumed to be driven by the temperature difference, and the latent heat transfer is assumed to be driven by the humidity difference. In this method, the sensible heat transfer coefficient is obtained from the sensible heat alone. This model was proposed by McQuiston.[2]

For the wet surface, the fin efficiency calculation requires heat and mass transfer analysis. The literature shows two fin efficiency models – enthalpy model and humidity model. The enthalpy model assumes that the heat and mass transfer between air and fin is driven by a enthalpy difference. This model is in line with the single potential model. In the humidity model, the latent heat transfer is linked with the sensible heat transfer by a humidity-temperature relationship. The enthalpy model has been used by ARI, and the humidity model was proposed by McQuiston.[2]

One simple and definitive method of comparing the heat and mass transfer models is to reduce sensible heat transfer coefficients from the data taken at different humidities. Consid-

Table 1 Previous studies on wet surface heat transfer of fin-and-tube heat exchangers

Investigators	Heat and mass transfer	Wet fin efficiency	Fin shape	Row	Fin pitch (mm)	Result
McQuiston[3]	Dual	Humidity	Plain	4	1.81~6.35	$h_d > h_w$ ($P_f > 3.172$ mm) $h_d \simeq h_w$ ($P_f \leq 3.172$ mm)
Wang et al.[4]	Single	Enthalpy	Plain	2, 4, 6	1.82~3.2	$h_d \simeq h_w$
Eckels and Rabas[5]	Single	Enthalpy	Wavy	3	1.97~3.13	$h_w > h_d$
Mirth et al.[6]	Single	Enthalpy	Wavy	4, 8	1.61~3.2	$h_d \simeq h_w$
Hong and webb[7]	Dual	Humidity (Wu&Bong modification)	Wavy lanced louver	2, 3	1.49~2.12	$h_d > h_w$

ering that forced convection heat transfer coefficients are not dependent on driving potentials such as temperature or humidity, an appropriate heat and mass transfer model will yield humidity-independent heat transfer coefficients.

The literature shows contradictory trends for the relative magnitude of the wet surface heat transfer coefficients (h_w) and the dry surface heat transfer coefficients (h_d). Existing studies are summarized in Table 1. McQuiston[3] tested four row plain fin samples, and reported that h_d was larger than h_w for $P_f > 3.175$ mm. For the smaller fin pitches, h_d was approximately the same as h_w. McQuiston[3] used the dual-potential model for the heat and mass transfer analysis, and the humidity model for the fin efficiency calculation. Wang et al.[4] tested plain fin heat exchangers of 2, 4 and 6 row configuration, and reported that h_d was approximately the same as h_w. They used the single-potential model for the heat and mass transfer analysis, and the enthalpy model for the fin efficiency calculation. Additional data on wave fin configuration[5-7] shown in Table 1 show contradictory trends, probably due to the different heat and mass transfer, and fin efficiency models.

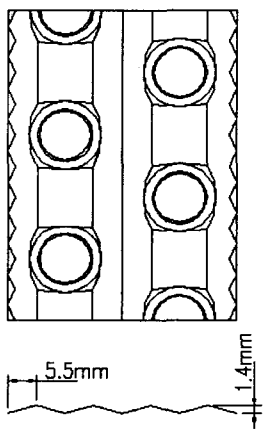

Fig. 1 Shape of the wave fin.

In this study, wet surface heat transfer tests were conducted for two heat exchangers (one with plain fin and the other with wave fin), and the data were reduced using two different heat and mass transfer models (single or dual enthalpy) and two different fin efficiency models (enthalpy or humidity), respectively. Figure 1 shows the wave fin configuration. Geometric details of the samples are listed in Table 2. The fin surface was hydrophilic-coated to facili-

Table 2 Heat exchanger samples

Sample	D_c[mm]	Fin shape	P_t[mm]	P_l[mm]	P_f[mm]	t_f[mm]	N	x_f[mm]	P_d[mm]
1	7.3	plain	21	12.5	1.49	0.115	2	-	-
2	10.3	wave	25.4	22	1.49	0.15	2	1.4	5.5

tate the condensate drainage. Dry-surface heat transfer tests were also conducted.

2. Experimental apparatus and test procedures

2.1 Experimental apparatus

A schematic drawing of the apparatus is shown in Fig. 2. It consists of a suction-type wind tunnel, water circulation and control units, and a data acquisition system. The apparatus is situated in a constant temperature and humidity chamber. The air-side inlet condition of the heat exchanger is maintained by controlling the chamber temperature and humidity. Dry and bulb temperatures in the inlet and the outlet are measured by the sampling method as suggested in ASHRAE Standard 41.1.[8] A diffusion baffle is installed behind the test sample to mix the outlet air. The water-side inlet condition is maintained by regulating the flow rate

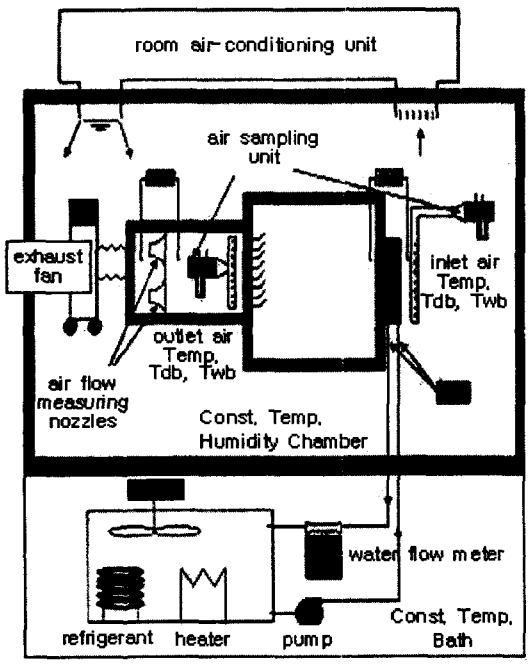

Fig. 2 Schematic drawing of the experimental setup.

and inlet temperature of the constant temperature bath situated outside of the chamber. Both the air and the water temperatures are measured by pre-calibrated RTDs (Pt-100Ω sensors). Their accuracies are ±0.1℃. The water flow rate is measured by a positive displacement type flow meter, whose accuracy is ±0.0015 liter/s. The air-side pressure drop across the heat exchanger is measured using a differential pressure transducer. The air flow rate is measured using a nozzle pressure difference according to ASHRAE Standard 41.2.[9] The accuracy of the differential pressure transducers is ±1.0 Pa.

The chamber temperature was maintained at 27℃ with 60% RH for wet surface tests, and 21℃ with 50% RH for dry surface tests. Experiments were conducted varying the frontal air velocity from 0.75 m/s to 2.5 m/s. The energy balance between the air-side and the tube-side was within ±3%. The discrepancy increased as the air velocity decreased. All the data signals were collected and converted by a data acquisition system (a hybrid recorder). The data were then transmitted to a personal computer for further manipulation. An uncertainty analysis was conducted following ASHRAE Standard 41.5,[10] and the results are listed in Table 3. The major uncertainty on the friction factor was the uncertainty of the differential pressure measurement (±10%), and the major uncertainty on the heat transfer coefficient (or j factor) was that of the tube-side heat transfer coefficient (±10%). The uncertainties decreased as the Reynolds number increased.

Table 3 Experimental errors

Parameter	Max. uncertainties
Temperature	±1.0℃
Differential pressure	±1.0 Pa
Water flow rate	$\pm 1.5\times10^{-6}$ m^3/s
Re_{Dc}	±2%
f	±10%
j	±12%

3. Data reduction methods

3.1 Dry surface

For the present cross-counter water-side circuits, the ε-NTU relationship is[11]

$$UA = \{(\dot{m}c_p)_{air} NTU_2\} \tag{1}$$

$$NTU_2 = -2\ln(1-K) \tag{2}$$

here, K is obtained from

2 row

$$\frac{K}{2} + \left(1-\frac{K}{2}\right)\exp(2KR) = \frac{1}{1-RP} \tag{3}$$

3 row

$$K\left[1-\frac{K}{4}-RK\left\{\left(1-\frac{K}{2}\right)\right\}\right]\exp(KR) + \left\{\left(1-\frac{K}{2}\right)\right\}^2\exp(3KR) = \frac{1}{1-RP} \tag{4}$$

where

$$R = \frac{T_{r,in}-T_{r,out}}{T_{air,in}-T_{air,out}} \tag{5}$$

$$P = \frac{T_{air,out}-T_{air,in}}{T_{r,in}-T_{air,out}} \tag{6}$$

For a 1-row configuration, cross-flow ε-NTU relationship is used. The air-side heat transfer coefficient is obtained from Eq. (7).

$$\frac{1}{\eta_o h_o A_o} = \frac{1}{UA} - \frac{1}{h_i A_i} - \frac{t}{kA_t} \tag{7}$$

The tube-side heat transfer coefficient is obtained from appropriate correlations. For the present smooth tube, Gnielinski[12] correlation was used. The surface efficiency η_o in Eq. (7) is obtained from

$$\eta_o = 1-\frac{A_f}{A_o}(1-\eta) \tag{8}$$

The fin efficiency is obtained from Schmidt[13] equation.

$$\eta = \frac{\tanh(m r_c \phi)}{m r_c \phi} \tag{9}$$

$$m = \sqrt{\frac{2h_o}{k_f t_f}} \tag{10}$$

$$\phi = \left(\frac{R_{eq}}{r_c}-1\right)\left[1+0.35\ln\left(\frac{R_{eq}}{r_c}\right)\right] \tag{11}$$

1 row

$$\frac{R_{eq}}{r_c} = 1.28\frac{P_t}{r_c}\left(\frac{\sqrt{(P_t/2)^2+P_l^2}}{P_t}-0.2\right)^{0.5} \tag{12}$$

2 row and more

$$\frac{R_{eq}}{r_c} = 1.27\frac{P_t}{r_c}\left(\frac{\sqrt{(P_t/2)^2+P_l^2}}{P_t}-0.3\right)^{0.5} \tag{13}$$

The heat transfer coefficient is expressed as the j-factor.

$$\mathrm{Re}_{Dc} = \frac{\rho_a V_{max} D_c}{\mu_a} \tag{14}$$

$$j = \frac{h_o}{\rho_a V_{max} c_{pa}} \mathrm{Pr}_a^{2/3} \tag{15}$$

The friction factor is obtained from

$$f = \frac{A_c}{A_o}\frac{\rho_m}{\rho_{in}}\left[\frac{2\Delta P \rho_{in}}{(\rho_m V_{max})^2} - (1+\sigma^2)\left(\frac{\rho_{in}}{\rho_{out}}-1\right)\right] \tag{16}$$

3.2 Wet surface (heat and mass transfer)

3.2.1 Single-potential model

Figure 3 shows the schematic drawing of the heat and mass transfer process occurring on dehumidifying surface. The heat transfer rate for the control surface dA becomes

$$dq = [h(T_a-T_s)+h_D(w_a-w_s)\{i_{wv}(T_a) - i_w(T_s)\}]dA \tag{17}$$

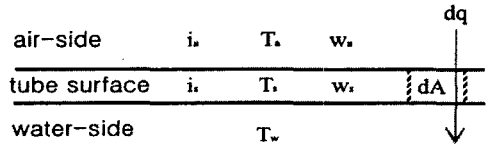

Fig. 3 A sketch illustrating the heat and mass transfer on the wet surface.

where h is the sensible heat transfer coefficient, and h_D is the mass transfer coefficient. The first term in Eq. (17) implies the sensible heat transfer, and the second term implies the latent heat transfer. The magnitude of $[i_{wv}(T_a) - i_w(T_s)]$ is approximately the same as latent heat of condensation i_{fg}.

$$dq = [h(T_a - T_s) + h_D(w_a - w_s) i_{fg}]\, dA \quad (18)$$

The mass transfer coefficient h_D is related with the heat transfer coefficient h as follows.

$$h_D = \frac{h}{c_{p_{ma}} \mathrm{Le}^{1-n}} \quad (19)$$

Here, n is the Prandtl number exponent, whose proper value is 1/3. Insertion of Eq. (19) into Eq. (18) yields

$$dq = \left[h(T_a - T_s) + \frac{h i_{fg}}{c_{p_{ma}} \mathrm{Le}^{1-n}} (w_a - w_s) \right] dA \quad (20)$$

Eq. (20) may be rearranged into

$$dq = \frac{h}{c_{p_{ma}}} \left[\left(c_{p_{ma}} T_a + \frac{i_{fg} w_a}{\mathrm{Le}^{1-n}} \right) - \left(c_{p_{ma}} T_s + \frac{i_{fg} w_s}{\mathrm{Le}^{1-n}} \right) \right] dA \quad (21)$$

The enthalpy of moisture-air mixture is

$$i_a = c_{p_{ma}} T_a + w_a i_{fg} \quad (22)$$

Insertion of Eq. (22) into Eq. (21) yields

$$dq = \frac{h}{c_{p_{ma}}} [(i_a - i_s) + (w_s - w_a) i_{fg} (1 - \mathrm{Le}^{n-1})]\, dA \quad (23)$$

the second term in Eq. (23) may be deleted without significant error (less than 3~4%).

$$dq = \frac{h}{c_{p_{ma}}} (i_a - i_s)\, dA \quad (24)$$

Eq. (24) implies that wet surface heat transfer is driven by the enthalpy difference between air and surface.

When enthalpy potential is the driving force, the definition of ε and NTU is different from those of the temperature driving system, and they are summarized in Table 4. Eqs. (1) and (2) should be changed accordingly.

$$UA = \dot{m}_a NTU_2 \quad (25)$$

Table 4 Definition of ε and NTU for wet surface heat transfer

	Sensible heat	Total heat	Latent heat
Driving potential	ΔT	Δi	Δw
Effectiveness (ε)	$\frac{Q_{sens}}{C_{min}(T_{r,in} - T_{a,in})}$	$\frac{Q_{tot}}{C_{min}(T_{a,in} - T_{r,in})}$	$\frac{Q_{tot}}{C_{min}(w_{a,in} - w_{s,in})}$
NTU	$\frac{UA}{C_{min}}$	$\frac{UA}{C_{min}}$	$\frac{UA}{C_{min}}$
C	$C_a = (\dot{m} c_p)_a$ $C_r = (\dot{m} c_p)_r$	$C_a = \dot{m}_a$ $C_r = \frac{(\dot{m} c_p)_r}{b_r}$	$C_a = \dot{m}_a i_{fg}$ $C_s = \dot{m}_a i_{fg} \frac{\Delta w_{air}}{\Delta w_{surface}}$

$$NTU_2 = -2\ln(1-K) \tag{26}$$

The K equations [Eqs. (3) and (4)] remain the same. However, R and P [Eqs. (5) and (6)] are re-defined using enthalpies instead of temperatures.

$$R = \frac{i_{r,in} - i_{r,out}}{i_{a,out} - i_{a,in}} \tag{27}$$

$$P = \frac{i_{a,out} - i_{a,in}}{i_{r,in} - i_{a,in}} \tag{28}$$

In Eqs. (27) and (28), i_r is the saturated air enthalpy at the tube-side water temperature. Once UA is obtained from an appropriate ε-NTU relation, the sensible heat transfer coefficient is calculated from Eq. (29).

$$\frac{b_{w,m}}{\eta_o h_w A_o} = \frac{1}{UA} - \frac{b_r}{h_i A_i} - \frac{b_t t}{k A_t} \tag{29}$$

Here, b_r, b_t, $b_{w,m}$ are the saturated-air enthalpy-temperature slope at the water, tube wall, and water film temperature, respectively.

3.2.2 Dual-potential model

McQuiston[2] divided the total heat transfer into sensible and latent parts. From Eq. (18),

$$dq = dq_s + dq_L \tag{30}$$

$$dq_s = h(T_a - T_s)\,dA \tag{31}$$

$$dq_L = h_D(w_a - w_s)\,i_{fg}\,dA \tag{32}$$

Sensible heat transfer is obtained from Eq. (33).

$$q_s = \dot{m}_a c_{p_a}(T_{a,in} - T_{a,out}) \tag{33}$$

The UA is obtained from the sensible heat transfer using Eqs. (1) to (6). The sensible heat transfer coefficient is calculated from Eq. (34).

$$\frac{1}{\eta_o h_w A_o} = \frac{1}{UA} - \frac{1}{h_i A_i} - \frac{t}{k A_t} \tag{34}$$

$$\eta_o = 1 - \frac{A_f}{A_o}(1-\eta_w) \tag{35}$$

3.3 Wet surface (fin efficiency)

3.3.1 Enthalpy model

Application of Eq. (24) to the control surface of the fin yields

$$dq = \frac{h}{c_{p_{ma}}}(i_a - i_{s,f})\,dA_f \tag{36}$$

The enthalpy difference in Eq. (36) is related with the temperature difference using m' in Eq. (37).

$$m' = \frac{i_a - i_{s,f}}{T_{wb,a} - T_{s,f}} \tag{37}$$

Here, $T_{wb,a}$ is the wet bulb temperature of the air. The m' is schematically drawn in Fig. 4. Insertion of Eq. (37) into Eq. (36) yields

$$dq = \frac{hm'}{c_{p_{ma}}}(T_{wb,a} - T_{s,f})\,dA \tag{38}$$

Ware and Hacha[14] proposed to replace m' by m'' of Eq. (39). The m'' implies the slope of enthalpy-saturation temperature curve at the fin average temperature. The m'' is schematically drawn in Fig. 4.

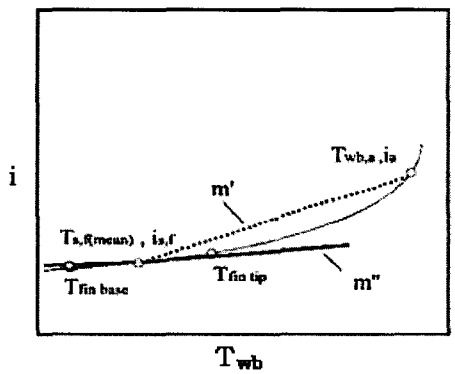

Fig. 4 Air enthalpy-saturation temperature curve illustrating m''.

$$m' \cong m'' \equiv \left[\frac{di}{dT}\right]_{T_{s,m}} \tag{39}$$

Insertion of Eq. (39) into Eq. (38) yields

$$dq = h_{eff}(T_{wb,a} - T_{s,f})\,dA \tag{40}$$

$$h_{eff} \equiv \frac{hm''}{c_{p_{ma}}} \tag{41}$$

Application of Eq. (40) into the control surface of the fin yields the following differential equation for the fin temperature.

$$\frac{d^2T}{dx^2} - \frac{h_{eff}P}{k_f A_c}(T_{wb,a} - T_f) = 0 \tag{42}$$

Eq. (42) is identical to the differential equation for the dry fin temperature, except that wet bulb temperature (instead of the dry bulb temperature) was used on the second term of the right-hand-side of the equation. Then, the wet surface fin efficiency becomes

$$\phi = \frac{\tanh(mL)}{mL} \tag{43}$$

$$m^2 = \frac{h_{eff}P}{k_f A_c} \cong \frac{2h_{eff}}{k_f t} \tag{44}$$

3.3.2 Humidity model

Application of Eq. (18) to the control surface of the fin yields Eq. (45).

$$\frac{d^2T_f}{dx^2} - \frac{hP}{k_f A_c}(T_f - T_a) - \frac{h_D P i_{fg}}{k_f A_c}(w_f - w_a) = 0 \tag{45}$$

To solve Eq. (45), McQuiston[2] introduced the C factor, which linearly relates the humidity and the temperature.

$$C \equiv \frac{w_f - w_a}{T_f - T_a} \tag{46}$$

Insertion of Eq. (46) into Eq. (45) yields Eq. (47).

$$\frac{d^2T}{dx^2} - M^2(T_f - T_a) = 0 \tag{47}$$

$$M^2 = \frac{hP}{k_f A_c}\left[1 + \frac{Ci_{fg}}{c_{p_{ma}}\mathrm{Le}^{1-n}}\right] \tag{48}$$

Figure 5 shows that the C value at the fin tip is different from that at the fin base. McQuiston[2] proposed to use fin-base C value for the entire fin surface. Wu and Bong,[15] Mirth and Ramadhyani[6] proposed improved models for the C.

The dual-potential model allows the calculation of the mass transfer coefficient h_D from the latent heat. The corresponding ε and NTU are summarized in Table 2.

$$q_{lat} = q - q_{sens} \tag{49}$$

$$h_D A = C_{air} NTU_2 \tag{50}$$

$$NTU_2 = -2\ln(1-K) \tag{51}$$

$$R = \frac{w_{s,in} - w_{s,out}}{w_{a,out} - w_{a,in}} \tag{52}$$

$$P = \frac{w_{a,out} - w_{a,in}}{w_{s,in} - w_{a,in}} \tag{53}$$

Here, w_s is the absolute humidity at the fin surface, and can be obtained from the thermal resistance ratio between the air-side and the water-side.

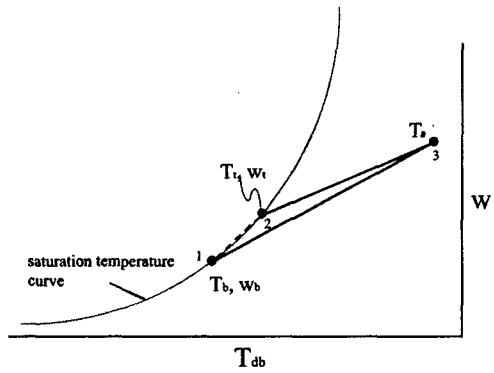

Fig. 5 Air humidity ratio-saturation temperature illustrating C.

4. Results and discussions

Two 2-row heat exchangers—one with plain fin, the other with wave fin—having 669 fpm (fins per meter) fin density were tested for $50\% \leq RH \leq 90\%$ ($T_{db}=27℃$). Figure 6 shows the plain fin j- and f-factors. Single-potential heat and mass transfer model was used for Figs. 6a and 6b. Fin efficiency models are different for Figs. 6a and 6b. Enthalpy fin efficiency model was used for Fig. 6a, and humidity fin efficiency model was used for Fig. 6b. For Figs. 6c and 6d, dual-potential heat and mass transfer model was used. Figure 6 shows that, when

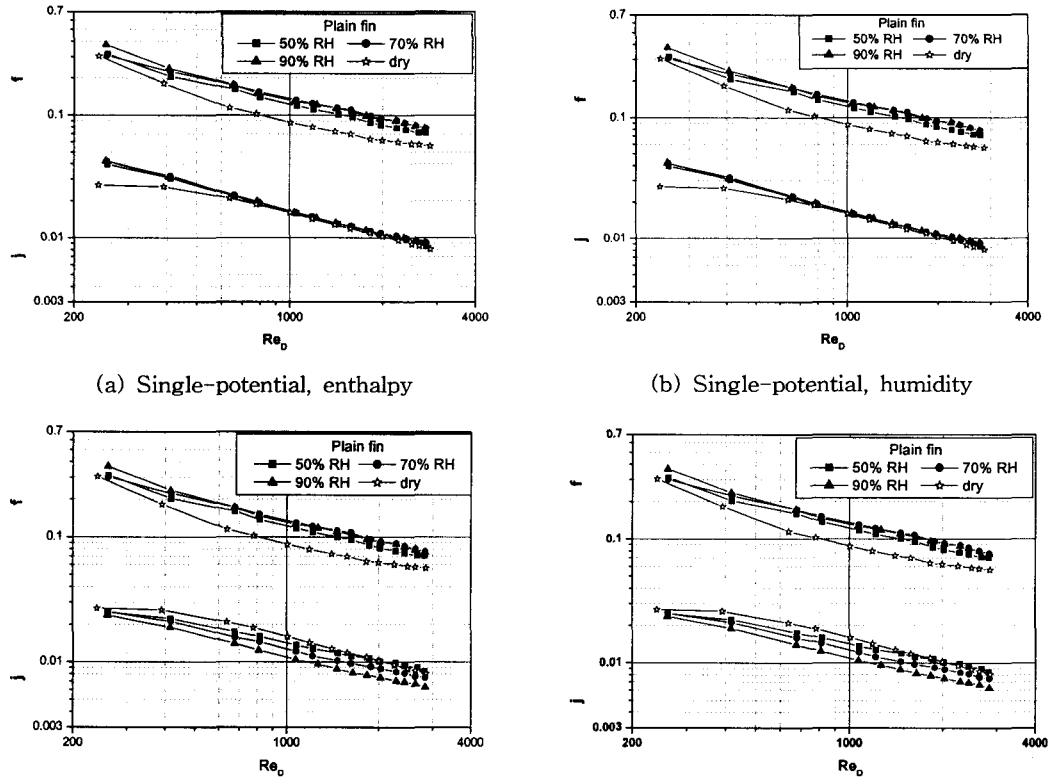

(a) Single-potential, enthalpy

(b) Single-potential, humidity

(c) Dual-potential, enthalpy

(d) Dual-potential, humidity

Fig. 6 The j- and f-factors showing the effect of relative humidity for the plain fin.

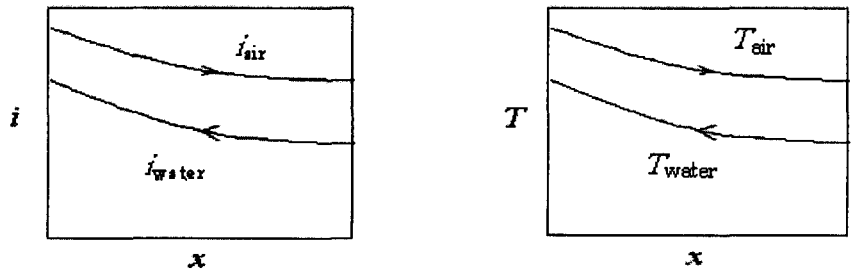

(a) Enthalpy

(b) Temperature

Fig. 7 Air and water property variation along the heat exchanger.

single potential model was used, the reduced j-factors are independent of the relative humidity. When dual-potential model was used, however, the reduced j-factors are smaller than those of the single potential model, and decrease as the relative humidity increases.

In the dual potential model, the heat transfer coefficient is reduced using the sensible heat transfer, i.e., the temperature difference between air and water stream. Figure 7 shows the enthalpy and the temperature variation along the heat exchanger. As shown in Fig. 7b, the water temperature increases by the heat transfer from the air. Both latent and sensible heat are transferred to water. However, the air temperature variation in Fig. 7b is caused by the sensible heat alone. This results in an imbalance of heat transfer. Thus calculated log mean temperature difference (LMTD) becomes larger than the actual LMTD, and accordingly, the reduced heat transfer coefficient becomes smaller. Mirth and Ramadhyani[6] also pointed out the problem of using temperature potential for the data reduction of the wet surface heat transfer. For the present study, the latent heat ratio (to the total heat) was 10% to 70%, increasing with the relative humidity. When enthalpy difference is used for the reduction of heat transfer coefficient as shown in Fig. 7a, the heat transfer between the air-side and the water-side is balanced.

The fin efficiency was reduced from the experimental data for the four cases, and the results are shown in Fig. 8. Figures 8a and 8b are for the single potential model, and 8c and 8d are for the dual potential model. The wet

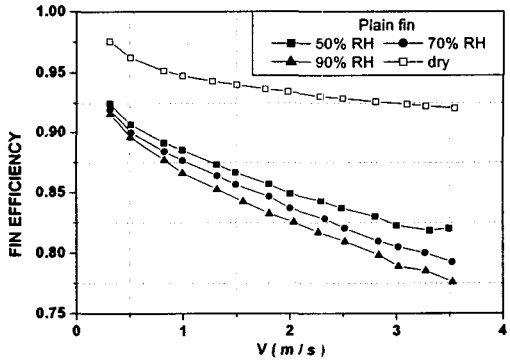

(a) Single-potential, enthalpy

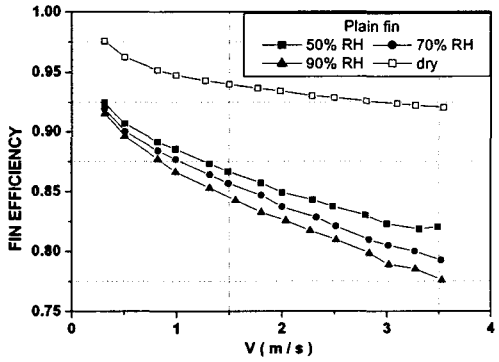

(b) Single-potential, humidity

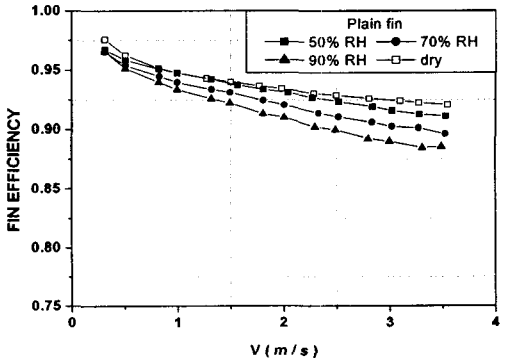

(c) Dual-potential, enthalpy

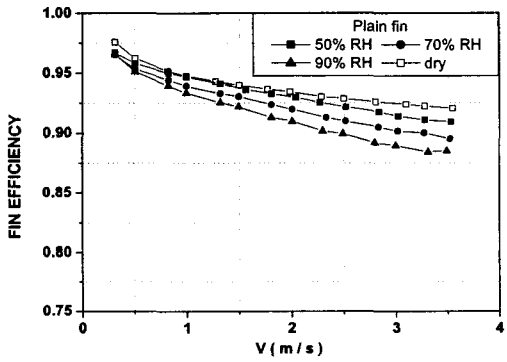

(d) Dual-potential, humidity

Fig. 8 Fin efficiency showing the effect of relative humidity for the plain fin.

surface fin efficiency is lower than that of the dry surface. The difference is less pronounced for the dual potential model. As discussed previously, the heat transfer coefficients reduced using dual potential model are smaller than those of single potential model. Smaller heat transfer coefficient yields larger fin efficiency. Existing studies on wet surface fin efficiency[2,15-17] also report significant decrease of the wet surface fin efficiency compared with those of the dry surface. Figure 8 shows that the fin efficiency decreases as the relative humidity increases. As the relative humidity increases, the condensate thickness increases, which results in decreased fin efficiency. Existing studies report that the fin efficiency is almost independent of the relative humidity when enthalpy model is used, and that the fin efficiency decreases as the relative humidity increases when humidity model is used. The present results show that fin efficiency models yield negligible difference in reduced fin efficiencies.

In Fig. 9, the dry surface f- and j-factors are also shown. The single-potential model results (Figs. 9a and 9b) show that dry surface j-factors are approximately the same as the wet surface j-factors for $Re_D > 1{,}000$. For lower Re_D, however, wet surface j-factors are higher. In addition, the wet surface j-factors continue to increase as the Reynolds number decreases. The dry surface j-factors tend to decrease at

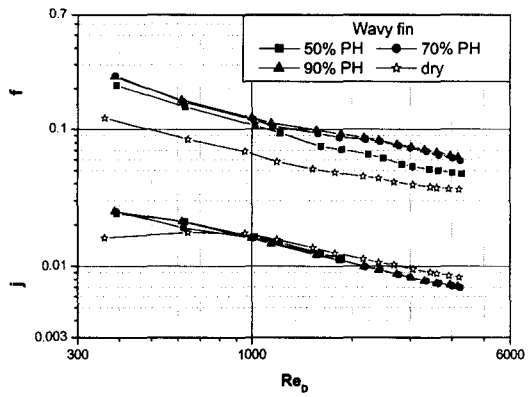

(a) Single-potential, enthalpy

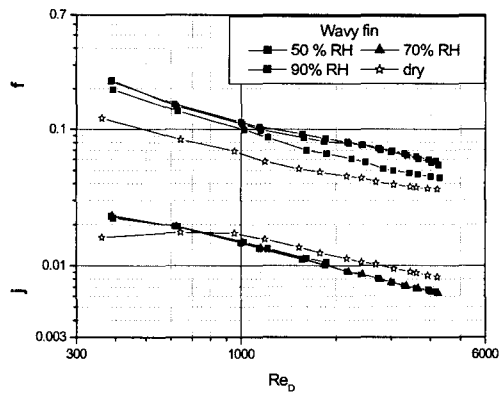

(b) Single-potential, humidity

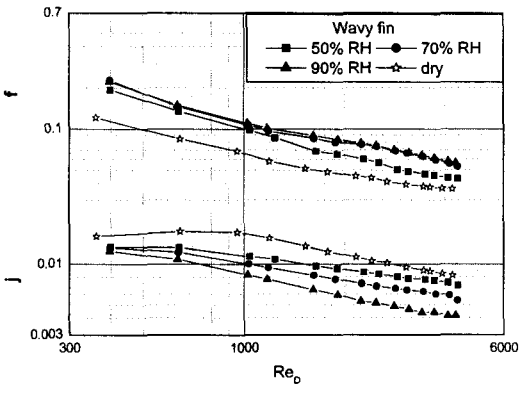

(c) Dual-potential, enthalpy

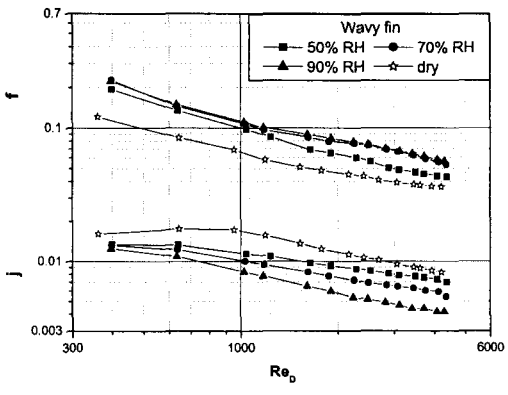

(d) Dual-potential, humidity

Fig. 9 The j- and f-factors showing the effect of relative humidity for the wave fin.

low Reynolds numbers. As reported by Wang et al.,[4] liquid drops hanging under the tube for a dehumidifying heat exchanger disturb the downstream flow, and the j-factor continues to increase as the Reynolds number decreases. The pressure drop increase for the wet surface compared with the dry surface was 10% to 35%. The pressure drop increases as the relative humidity increases, with 11% to 30% increase for 90% RH compared with those for 50% RH. The air flow area decreases with increasing relative humidity, due to the increased condensate thickness.

In Fig. 9, the wet surface heat transfer coefficients of the wavy fin heat exchanger are shown. Similar to the plain fin case, the heat transfer coefficients are independent of the relative humidity when the single potential model was used. The wet surface j-factors are 12% lower than the dry surface j-factors. The wet surface pressure drops are 25% to 45 % higher than the dry surface values. The pressure drop increases as the relative humidity increases, with 7% to 15% increase for 90% RH compared with those for 50% RH.

5. Conclusions

Four different methods of reducing the heat transfer coefficients from experimental data under dehumidifying conditions are compared. The four methods consist of two heat and mass transfer models and two fin efficiency models. Data are obtained from two heat exchanger samples having plain fins and wave fins, respectively.

(1) Comparison of the reduced heat transfer coefficients revealed that the single potential heat and mass transfer model yielded the humidity-independent heat transfer coefficients.

(2) Dual potential model is not recommended for wet surface data reduction, because only sensible heat is considered for the calculation of the heat transfer coefficient. This model is not appropriate except for case having very low latent heat ratio.

(3) Two different fin efficiency models—enthalpy model and humidity model—yielded approximately the same fin efficiency and accordingly approximately the same heat transfer coefficients.

(4) For the plain fin configuration, the wet surface heat transfer coefficient was approximately the same as the dry surface heat transfer coefficient. For the wavy fin configuration, the wet surface heat transfer coefficient was 12% lower than the dry surface value.

(5) The pressure drop was higher for the wet surface; 10% to 35% for the plain fin configuration, and 24% to 45% for the wavy fin configuration.

References

1. ARI 410-81, Standard for forced-circulation air-cooling and air-heating coils, American Refrigeration Institute.
2. McQuiston, F. C., 1975, Fin efficiency with combined heat and mass Transfer, ASHRAE Trans., Vol. 81, No. 1, pp. 350-355.
3. McQuiston, F. C., 1978, Heat, mass and momentum transfer data for five plate-fin-tube surfaces, ASHRAE Trans., Vol. 84, Part 1, pp. 266-293.
4. Wang, C.-C., Hsieh, Y.-C. and Lin, Y.-T., 1997, Performance of plate finned tube heat exchangers under dehumidifying conditions, J. Heat Transfer, Vol. 119, pp. 109-117.
5. Eckels, P. W. and Rabas, T. J., 1987, Dehumidification: on the correlation of wet and dry transport process in plate finned-tube heat exchangers, J. Heat Transfer, Vol. 109, pp. 575-582.
6. Mirth, D. R., Ramadhyani, S. and Hittle, D. C., 1993, Thermal performance of chilled water cooling coils at low water velocities, ASHRAE Trans., Vol. 99, Pt. 1, pp. 43-53.
7. Hong, K. and Webb, R. L., 1999, Perfor-

mance of dehumidifying heat exchangers with and without wetting coatings, J. Heat Transfer, Vol. 121, pp. 1018-1026.
8. ASHRAE Standard 41.1, 1986, Standard method for temperature measurement, ASHRAE.
9. ASHRAE Standard 41.2, 1986, Standard method for laboratory air-flow measurement, ASHRAE.
10. ASHRAE Standard 41.5, 1986, Standard measurement guide, engineering analysis of experimental data, ASHRAE.
11. Taborek, J., 1998, F and θ charts for cross-flow arrangements, in Heat Transfer Enhancement of Heat Exchangers, Eds., S. Kakac, A. E. Bergles, F. Mayinger, H. Yuncu, Kluwer Academic Press, pp. 141-162.
12. Gnielinski, V., 1976, New equations for heat and mass transfer in turbulent pipe flows, Int. Chem. Eng., Vol. 16, pp. 359-368.
13. Schmidt, T. E., 1949, Heat transfer calculations for extended surfaces, J. ASRE, Refrigeration Engineering, Vol. 4, pp. 351-357.
14. Ware, H. and Hacha, T., 1960, Heat transfer from humid air to fin and tube extended surface cooling coils, ASME Paper No. 60-HT-17.
15. Wu, G. and Bong, T. Y. 1994, Overall efficiency of a straight fin with combined heat and mass transfer, ASHRAE Trans., Pt. 1, Vol. 100, pp. 367-374.
16. Lin, Y. T., Hsu, K. C., Chang, Y. J. and Wang, C. C., 2001, Performanace of rectangular fin in wet conditions: visualization and wet fin efficiency, J. Heat Transfer, Vol. 123, pp. 827-836.
17. Hong, K. and Webb, R. L., 1996, Calculation of fin efficiency for wet and dry fins, Int. J. HVAC & R Research, Vol. 2, No. 1, pp. 27-41.